# Can the Last Interglacial Constrain Projections of Future Antarctic Ice Mass Loss and Sea-level Rise?

**Daniel M. Gilford[1,2], Erica L. Ashe[2], Robert E. Kopp[1,2], Robert M. DeConto[3], David Pollard[4], Alessio Rovere[5]**

[1]Institute of Earth, Ocean, and Atmospheric Sciences, Rutgers University, 71 Dudley Road, Suite 205, New Brunswick, NJ 08901, USA.
[2]Department of Earth and Planetary Sciences, Rutgers University, Piscataway, NJ, USA.
[3]Department of Geosciences, University of Massachusetts, Amherst, MA, USA.
[4]Earth and Environmental Systems Institute, Pennsylvania State University, University Park, PA, USA.
[5]University of Bremen, Marum, ZMT, Bremen, Germany.

**Key Points:**

- Current last interglacial estimates do not meaningfully constrain future near-term Antarctic mass losses or processes, but they are more informative over time
- If last interglacial peak Antarctic contributions were known precisely, there would still be some uncertainty in projections of future ice-sheet mass losses
- Improved last interglacial field observations have potential to reduce future projection uncertainty, depending on the paleo sea level storylines considered

Corresponding author: Daniel Gilford, `daniel.gilford@rutgers.edu`

**Abstract**

Deep uncertainty in future Antarctic ice-sheet mass loss makes it challenging to produce robust projections of sea-level rise. Previous studies used peak last interglacial period (LIG; ∼129-116 ka) sea-level estimates to calibrate future projections of Antarctic mass loss. But LIG estimates have various depictions and interpretations across the literature. To what extent is the LIG able to inform future Antarctic contributions to sea-level rise? This study develops a Gaussian process emulator of an ice-sheet model to produce continuous probabilistic projections of Antarctic sea-level contributions over the LIG and a future high-emissions scenario. A Bayesian approach is used to condition emulator projections on a set of LIG constraints to find associated likelihoods of model parameterizations. Results show how LIG estimates inform (1) the mechanisms of past and future ice-sheet instabilities and (2) projections of future sea level rise through 2150. Best available LIG estimates do not meaningfully constrain future near-term Antarctic mass losses or physical processes. However, LIG estimates become more informative over time, as projections subject to ice-sheet instabilities become more positively skewed. Considerable uncertainties in future projections remain even if peak LIG Antarctic ice-sheet retreat is precisely known, indicating peak LIG changes are an imperfect analog for future ice-sheet sensitivities to climate warming. The efficacy of LIG constraints on Antarctic sea-level contributions also depends on assumptions about the Greenland ice sheet and LIG sea-level chronology. However, improved field measurements and understanding of LIG sea-levels still have potential to improve future sea-level projections, highlighting the importance of continued observational efforts.

## 1 Introduction

Coastal communities are facing increasing threats from sea-level rise, creating a growing need for comprehensive probabilistic projections (Kopp et al., 2014; Kopp, DeConto, et al., 2017; Horton et al., 2018) to inform coastal risks and adaptation practices (Buchanan et al., 2016, 2017; D. J. Rasmussen et al., 2018). The single largest source of uncertainty in $21^{st}$ century sea-level rise is the Antarctic ice sheet (AIS), with projected loss dependent on the ice-sheet physics considered, modeling and statistical methodologies, and observational constraints (e.g., Kopp, DeConto, et al., 2017).

There is deep uncertainty in future AIS sea-level contributions, meaning that their full probability distribution is unknown and cannot be estimated or agreed upon by experts (Lempert & Collins, 2007). This deep uncertainty is illustrated in the lack of agreement in the scientific community on projected probabilities of AIS contributions, which is partially related to unresolved challenges in modeling ice-sheet processes (Fuller et al., 2017; Bakker, Wong, et al., 2017; Bakker, Louchard, & Keller, 2017; Bamber et al., 2019). There is a growing consensus that the AIS is threatened by marine ice-sheet instability (MISI; Weertman, 1974; Schoof, 2007), which would lead to accelerated mass loss irreversible on millennial scales (Golledge et al., 2015; Bulthuis et al., 2019) and skew probability distributions towards fat upper-tails in sea-level projections (Robel et al., 2019). There is some evidence that MISI is already underway in the Thwaites/Pine Island Glacier basins (Joughin et al., 2014; Favier et al., 2014), and western AIS ice discharge has accelerated in recent years (Gardner et al., 2018; Rignot et al., 2019). But more uncertain is the role of marine ice-cliff instability (MICI), which was proposed as a primary loss mechanism by DeConto and Pollard (2016). MICI is not well understood and is difficult to parameterize (Bassis & Walker, 2012). While it has not yet been observed in Antarctica, there are modern examples of cliff instability seen in Greenland glaciers (DeConto & Pollard, 2016; Parizek et al., 2019) and new iceberg-keel plough mark evidence for MICI in Pine Island Bay in the early Holocene, ∼12,000 years before present (Wise et al., 2017). However, a recent reanalysis of DeConto and Pollard (2016) has shown that the MICI mechanism is not well constrained, and is unnecessary for ice-sheet model projections

to be consistent with modern observations and paleoclimate estimates of AIS mass loss (Edwards et al., 2019).

A major challenge for constraining future projections of AIS sea-level contributions is the information gap between what has been observed and what could occur. The world is facing unprecedented climate forcing and warming (Stocker et al., 2013). Although there is ongoing global progress to reduce human emissions and the resulting climate change, there are already substantial commitments to irreversible warming and thermosteric sea-level rise (Meehl et al., 2005; Solomon et al., 2009; Zickfeld et al., 2017). The Antarctic ice sheet is also committed to mass loss this century (Mengel et al., 2016, 2018), and parts of western AIS may already be on a path toward collapse even without any additional forcing (Arthern & Williams, 2017). Whether or not major ice-sheet discharge will occur through MICI is critical for future outcomes and impacts on human systems (Oppenheimer & Alley, 2016; Wong et al., 2017; Stammer et al., 2019). However, because there are little or no significant correlations between observed trends and potentially nonlinear future large-scale ice-sheet loss (Kopp, DeConto, et al., 2017), modern observations are inadequate for constraining whether MICI will be a primary driver of sea-level rise. Instead, the information gap must be filled with analogs from the past, specifically through the paleoclimate sea-level record. The last interglacial (LIG) period has been invoked as a relevant constraint on ice-sheet instability processes (including MICI) and model projections (DeConto & Pollard, 2016; Steig & Neff, 2018), but it is not clear how informative it is. In this study we investigate how interpretations and estimates of AIS sea-level contributions during the LIG may be combined with ice-sheet model ensembles to inform and improve probabilistic projections of future sea-level rise.

The last interglacial (∼129,000 to 116,000 years before present, ka) was a period of higher orbital eccentricity, slightly above average global mean temperatures, and substantial warming in polar atmospheric temperatures (>3°C warmer than present) and high-latitude ocean temperatures (1°C warmer than present) (Capron et al., 2017, and references therein). Accompanying this were estimated global mean sea levels (GMSL) about 6–9 m higher than present (Dutton, Carlson, et al., 2015), driven by a combination of mountain glacial melt, Greenland and Antarctic ice-sheet mass loss contributions, and thermosteric effects. While the proportional mix of these contributions is uncertain, previous studies have determined that some portion of the Antarctic ice sheet (and likely primarily the less stable western AIS) retreated during the LIG (e.g., Scherer et al., 1998; Dutton, Carlson, et al., 2015; Dutton, Webster, et al., 2015). The LIG has long been an analog for considering AIS contributions to sea-level rise in warm climates (Mercer, 1968; Hansen et al., 1981). But although the LIG is potentially useful for constraining the sensitivity of ice sheets in a warmer world, the LIG may not be an ideal analog for future climate changes, because its forcing is driven by fundamentally different mechanisms (Capron et al., 2019).

Estimates of AIS sea-level contributions during the LIG have their own deep uncertainty. Different interpretations and applications of paleo sea level estimates have led to divergent projections and conclusions about what instability processes could drive future sea-level rise (cf. DeConto and Pollard (2016) and Edwards et al. (2019)). The goal of this study is to analyze the extent to which the LIG can inform future projections, given the inherent uncertainties in ice-sheet processes and LIG estimates. One outcome is an explicit comparison between future projections conditional on LIG estimate distributions which have been previously (or could be) used to calibrate ice-sheet models. Furthermore, our methodology allows us to explore how different assumptions about the AIS LIG sea-level evolution influences the modeling of future sea-level changes. This analysis provides useful targets and research directions for the paleo sea level observational community.

It is not feasible to produce sufficient model simulations for comprehensive statistical analyses, because ice-sheet model runs are computationally expensive, sparsely con-

structed across the model parameter space, and discrete. We instead develop a statistical "emulator" to fill intermediate solutions that have not been simulated (Kennedy & O'Hagan, 2001; C. E. Rasmussen & Williams, 2006). The emulator is designed to mimic the behavior of the simulator at any combination of model parameters within the range of the training simulations (Bastos & O'Hagan, 2009; Edwards et al., 2019). We emulate ice-sheet model simulations of the LIG and the future ice-sheet evolution under a high-emissions scenario. The emulator provides a continuous estimate of AIS sea-level contributions over a range of model parameters. We sample from the emulator to perform Bayesian statistical analyses to investigate the dependencies of future Antarctic sea-level contributions on the LIG.

The intention of this study is not to produce a representative set of probabilistic projections describing the full range of uncertainties inherent in AIS contributions to sea-level rise. In fact, we posit that the utility of such projections is suspect without a full exploration of structural and parametric ice-sheet model uncertainties (e.g., Seiyon Lee et al., 2019). Instead we demonstrate how LIG constraints may inform sea-level projections in the context of specific parameter values for a single ice-sheet model. Our method is deliberately developed with a generalized and flexible framework that could be modified to analyze any carefully constructed ensemble of ice-sheet model simulations. This could include extensions to the Greenland ice sheet, other ice-sheet models or ensembles (e.g. ISMIP6, Nowicki et al. (2016); Goelzer et al. (2018)), different parameters or regions of parameter space, or different paleo sea level constraints (e.g. the Pliocene).

Section 2 provides a detailed overview of the ice-sheet model ensembles used to train the emulator, the emulation methodology, the Bayesian approach, and the LIG constraints considered herein. Section 3 presents the study results, showing the importance of LIG estimates for future projections of Antarctic contributions to sea levels. In section 4 we discuss the implications of our findings for future research directions in the paleo sea level community. Concluding remarks are presented in section 5.

## 2 Models and Methods

### 2.1 Ice-sheet Simulations

We develop an emulator trained on two ensembles of ice-sheet model simulations: 1) the LIG, and 2) a future high emissions scenario. Simulations are run with a numerical ice-sheet model which has been used in several studies of ice-sheet contributions to past and future sea levels (Pollard & DeConto, 2009; DeConto & Pollard, 2016; Pollard et al., 2016, 2017; Kopp, DeConto, et al., 2017; Pollard et al., 2018; Edwards et al., 2019). The ice sheet model (Pollard & DeConto, 2012) uses vertically integrated shallow ice approximation-shallow shelf approximation ice dynamics, and migrating grounding lines and floating ice shelves with parameterized grounding-line flux (Schoof, 2007). Hydrofracturing due to surface melt and structural failure of tall ice cliffs are included (Pollard et al. (2015); DeConto and Pollard (2016), discussed more below). Internal ice temperatures are simulated, with basal sliding and sediment deformation occurring only where the base is at or near the melt point, and no explicit basal hydrology. A Weertman-type basal sliding law over bedrock is used with sliding velocity proportional to the square of basal shear stress, and spatially dependent coefficients (Pollard & DeConto, 2012).

The model simulations used in this study are an improvement on those presented in DeConto and Pollard (2016) and reanalyzed in Edwards et al. (2019). In particular, model runs use enhanced model physics for sub-oceanic melt-rates, runs have a reduced bias correction on sub-surface oceanic temperatures, and atmospheric and oceanic forcing conditions are applied synchronously in the future simulations.

LIG equilibrium model simulations are forced by representative oceanic and atmospheric conditions from 130 ka constructed from a synthesis of paleoclimate reconstruc-

tions and climate-modeling (Capron et al., 2014). The simulations are run for 5000 years to bring them approximately into equilibrium with these forced climate conditions, and we take the final (year 5000) values as representative of the peak AIS mass loss response during the LIG. Emulated peak LIG changes are paired with reconstructed sea-level estimates in our study to assess the efficacy of the LIG for influence future projections of AIS contributions to sea-level rise (section 2.2-2.4).

Future transient simulations used in this study span 1990-2150 and are forced by time-evolving atmospheric and ocean conditions from a high-emissions scenario (Representative Concentration Pathway 8.5, RCP8.5; Riahi et al. (2011)). We report future AIS sea-level contributions relative to the year 2000.

In both LIG and future simulations, ensembles are constructed by varying two model parameters—CREVLIQ and CLIFVMAX—over 14 discrete values each to produce 196 members (Supporting Information Table S1). *CREVLIQ* is the proportional sensitivity of model hydrofracturing to surface liquid, i.e. from rain and meltwater ($\frac{m}{(myr^{-1})^2}$, see Eqn. B6 in Pollard et al. (2015)). As CREVLIQ increases, ice-sheet crevasses deepen more readily in response to surface liquid accumulation, which increases the chance of hydrofracturing and removal of buttressing ice shelves. *CLIFVMAX* is the maximum rate ($\frac{km}{yr}$) of horizontal cliff wastage once an ice cliff becomes mechanically unstable and collapses (i.e. under MICI). As CLIFVMAX increases, structurally unstable ice cliffs may retreat at a rate up to the increased bound. Note that when CLIFVMAX=0 $\frac{km}{yr}$, ice cliffs cannot retreat even when they would theoretically fail; in this set of simulations MICI is effectively turned off.

Ensemble timeseries of AIS mass loss in sea level equivalent (SLE) from the LIG and RCP8.5 scenarios are shown in Figure 1; curves depicting the evolution of the ensemble members are color-coded by CLIFVMAX values. For reference, in Fig. 1a we show the estimated range of AIS contributions to GMSL during the LIG which was assumed by DeConto et al. (2019) and based on reconstructions described in Dutton, Carlson, et al. (2015) (see section 2.4).

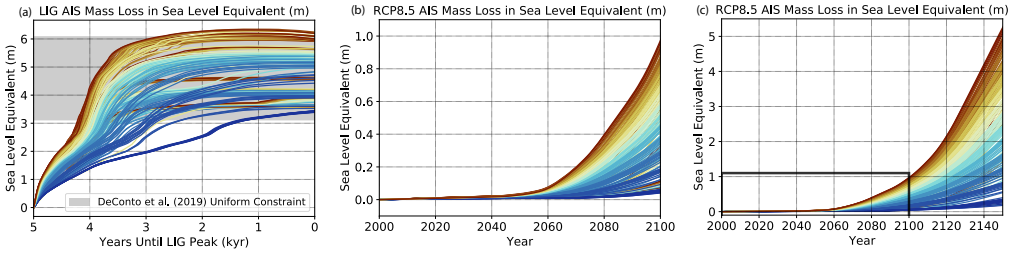


**Figure 1.** Timeseries of simulated mass losses in sea-level equivalent (m) from the AIS (a) during the LIG and (b-c) projected under an RCP8.5 scenario over 2000-2150. (b) is identical to (c), except it is zoomed in over 2000-2100. Simulated timeseries are color-coded by their CLIFVMAX values from 0 $\frac{km}{yr}$ (dark blue) to 13 $\frac{km}{yr}$ (red). Gray shading in (a) is the range of LIG AIS sea-level contribution constraints estimated in DeConto et al. (2019).

The evolution of LIG simulations (Fig. 1a) suggests that there are distinct ice mass loss events (e.g. the acceleration of sea-level contributions in some simulations ∼1000 years into the simulation) in response to constant forcing, and their occurrence depends strongly on model parameter values. This nonlinear behavior results in a multi-modal distribution of the ensemble's peak AIS mass loss (discussed further in section 3). AIS discharge is sensitive to the value of CLIFVMAX on the timescale of centuries, as seen in the first 1000 years of the LIG ensemble and the entirety of the RCP8.5 simulation

(Fig. 1b-c). The non-monotonic color progression of LIG timeseries in Fig. 1a shows that under orbital forcing and on millennial timescales CREVLIQ plays a more substantial role in ice-sheet mass loss (cf. Supporting Information Figure S1).

Future simulations of mass loss under RCP8.5 forcing are very similar across the ensemble in the early $21^{st}$ century; 158/196 simulations have loss rates consistent with IMBIE2 estimates over 1992-2017 (15-46 $\frac{mm}{yr}$); IMBIE-Team (2018)). Ice discharge begins to dramatically accelerate among ensemble members with higher CLIFVMAX values, and simulations markedly diverge around 2060. Ice loss continues to accelerate across the simulations through the end of the century and until about 2150. By 2150, the median rate of sea level equivalent mass loss among ensemble members is 54 $\frac{mm}{yr}$, and 50% of the simulations have lost at least 2.3 m of ice in sea level equivalent. Mean RCP8.5 ensemble AIS sea level contributions are 42 cm in 2100 and 2.3 m 2150. These are lower than DeConto and Pollard (2016) large-ensemble projections in both 2100 (77 cm) and 2150 (2.9 m).

These ice-sheet model ensembles have notable structural limitations. They are constructed over only two model parameters, whereas there are >10 unique parameters not explored here (held constant) and which could influence sea-level contributions from Antarctica (Pollard et al., 2015) (e.g., the oceanic melt factor, basal sliding coefficients, the timescale of isostatic rebound, etc.). The full sensitivity of this ice-sheet model to its model parameters is an area of active research (Seiyon Lee et al., 2019). Another limitation is the choice of the prior ranges for CREVLIQ and CLIFVMAX: although the values in these ranges are relatively densely sampled (Supporting Information Table S1), there is no information beyond these values, and the emulator will not be applicable outside of these ranges (section 2.2). The emulator is also trained with simulations from the single ice-sheet model, and thus any structural model uncertainties will be inherent in our emulator. Because our goal is to illustrate how LIG constraints influence sea-level projections (rather than fully describe the deep uncertainties in AIS contributions to sea-level rise), we consider these ensembles to be sufficient for these purposes.

### 2.2 Emulation

The emulator is trained separately on the 196-member last interglacial and RCP8.5 ensembles ($\mathbf{z_{LIG}}$ and $\mathbf{z_{RCP}}$, respectively) using Gaussian process (GP) regression (C. E. Rasmussen & Williams, 2006; Ashe et al., 2019). We model the total Antarctic ice sheet contributions to global mean sea level $[f(\theta_1, \theta_2, t)]$ as the sum of two terms, each with a zero-mean GP prior distribution:

$$f(\theta_1, \theta_2, t) = f_1(\theta_1, \theta_2) + f_2(\theta_1, \theta_2, t) \tag{1}$$

The first term $[f_1(\theta_1, \theta_2)]$ represents a time-independent function across the ensemble's model parameter space $[\theta_1, \theta_2]$, and the second term $[f_2(\theta_1, \theta_2, t)]$ is the contribution with temporal evolution. We specify the prior distributions of each term as:

$$f_1(\theta_1, \theta_2) \sim \mathcal{GP}(0, \alpha_1^2 K(\theta_1, \theta_2, \theta_1', \theta_2'; \ell_1)) \tag{2}$$

$$f_2(\theta_1, \theta_2, t) \sim \mathcal{GP}(0, \alpha_2^2 K(\theta_1, \theta_2, \theta_1', \theta_2', \ell_2) \cdot K(t, t'; \tau)) \tag{3}$$

where $\theta_1$ and $\theta_2$ are the values of CLIFVMAX and CREVLIQ normalized by their respective maximum values in the simulator ensemble parameter space (Supporting Information Table S1), $\alpha_i$ are prior standard deviations, $\ell_i$ are characteristic length scales in normalized parameter space, $\tau$ is the characteristic time scale and $K$ is a specified correlation function. Because the LIG training data are evaluated at a single time point, there is no temporal term and $f_2$ is excluded in the LIG emulator construction. $K$ is defined to be a Matérn covariance function with a specified smoothness parameter, $\gamma$, which

governs how responsive the covariance function is to sharp changes in the training data (C. E. Rasmussen & Williams, 2006). The choice of the Matérn covariance function allows for non-parametric nonlinear behavior in time and space. For the RCP8.5 scenario $\gamma = \frac{5}{2}$ because transient sea-level contributions vary smoothly across the model parameter space and time; for the LIG scenario, $\gamma = \frac{1}{2}$, because peak LIG sea-level contributions vary more sharply across the model parameter space.

Optimal hyperparameters ($\alpha_i$, $\ell_i$, and $\tau$) of the GP model are found by maximizing the model's likelihood, given the training simulations (Supporting Information Table S2, C. E. Rasmussen and Williams (2006)). The "nugget" (point-wise variance) of the optimized emulator is specified as $10^{-6}$ because the simulator is deterministic, and therefore the emulated mean should approximately match the training ensemble data at each input across the parameter space and time. The optimized emulator is then conditioned on the training ensembles (i.e. $f|\mathbf{z}$) to predict continuous sea-level contributions for LIG and RCP8.5 at parameter values and times between the discrete simulator predictions of the full ice-sheet model. We refer to this optimized model as the "prior" emulator. We performed leave-one-out analysis to validate the optimized prior emulator following Bastos and O'Hagan (2009) and found it accurately mimics the behavior of the ice-sheet simulator over LIG and RCP8.5 scenarios (see Supporting Information, Text S1, Fig. S2–S3).

Figure 2 shows the emulator prior mean functions (background contours) and corresponding training simulations (circles) for the LIG and RCP8.5 in 2100 across the model's parameter space. For reference, contours of the two training ensembles are plotted against each other in Supporting Information Figure S1. There are some similarities between the simulated sea levels during the LIG and those projected over the coming century under RCP8.5. In both ensembles, sea-level contributions increase as the model becomes more sensitive to retreat following ice-cliff collapse or hydrofracturing. Sea-level projections are also substantially lower when either CREVLIQ or CLIFVMAX are zero; physically, these parameterizations are equivalent to either hydrofracturing from surface melt/precipitation or mechanically unstable cliff retreat, respectively, being turned off. The gradients transitioning from these ensemble members to those where CREVLIQ/CLIFVMAX $> 0$ are relatively steep, demonstrating that these processes are relevant and primary drivers of both future projections and calibration with paleo estimates (see section 2.3).

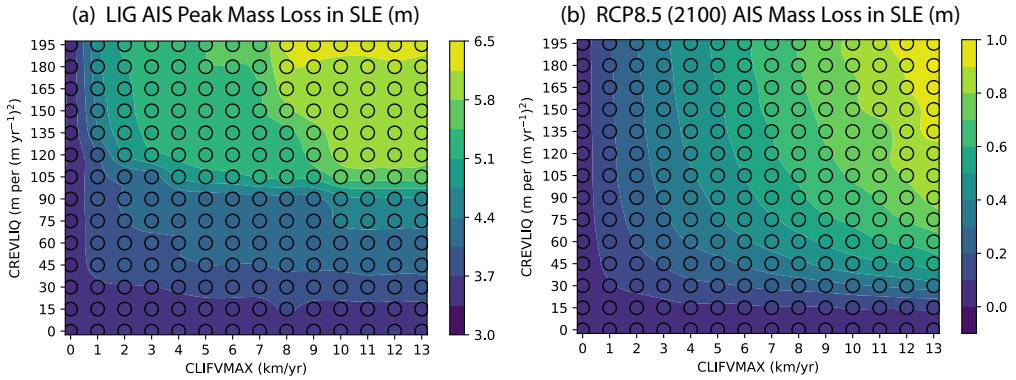


**Figure 2.** Simulated (filled circles) and mean emulated (contours) sea-level contributions from the Antarctic ice sheet across the model's prior ensemble parameter space (a) during the last interglacial, and (b) projected under an RCP8.5 scenario in 2100.

There are also differences between the two training ensembles. In particular, future projection simulations have a stronger gradient along CLIFVMAX and quickly be-

come insensitive to changes along CREVLIQ. This result becomes more pronounced throughout the early $22^{nd}$ century (not shown). In contrast, LIG sea-level contributions from the AIS are sensitive to both CREVLIQ and CLIFMVAX in some regions of the parameter space, but are nearly constant across parameter changes in other regions (e.g. where CREVLIQ $> 120$ and $2 <$ CLIFVMAX $< 7$). These regions highlight that with prolonged fixed forcing different sectors of ice can be completely lost and their sea-level contributions can cluster across a broad range of parameter values. It then takes more parameterized sensitivity to forcing to reach the next stage of significant mass loss, as shown by the acceleration in mass loss that spontaneously occurs in the LIG ensemble timeseries (Fig. 1a). This behavior is much less pronounced over the relatively short modern period of transient and increasing forcing, as shown by its smoothly varying sea-level contributions (Fig. 1c). These scenario differences have important implications for projection calibrations. They imply that even if the LIG contributions were known exactly, depending on the region of parameter space the estimates fell into there may be a limit to how much the LIG could constrain future projections (discussed in section 3).

Having developed a prior emulator trained and conditioned on each training ensemble, we sample it with a Latin-hypercube design of 10,000 points over the parameter space. The timeseries of these samples from the RCP8.5 emulator prior distribution are shown in Figure 3.

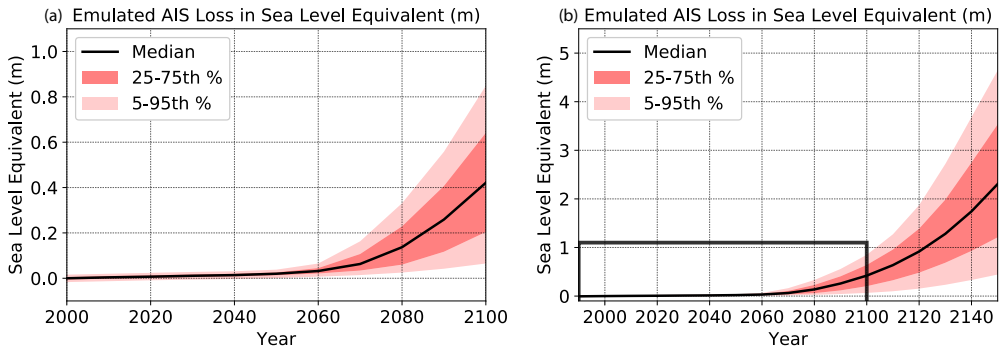


**Figure 3.** Emulator prior probability distributions of AIS mass loss in sea-level equivalent (m) projected under the RCP8.5 scenario over 2000-2150. (a) is identical to (b), except it is zoomed in over 2000-2100. Shown are the median (solid black line), $25^{th} - 75^{th}$ (red shading), and $5^{th} - 95^{th}$ percentiles (light red shading).

### 2.3 Bayesian Updating

We use Bayesian updating to determine the influence of LIG constraints on future projections of Antarctic contributions to sea-level rise. Let $f_{RCP}$ be the future AIS sea-level contributions estimated by the emulator, and $y$ be a specified or known constraint of peak LIG AIS mass loss. We take a uniform prior over the input parameters $(\theta_1, \theta_2)$ across the full range of the ice-sheet model ensembles (Supporting Information Table S1).

We seek the probability distribution of future AIS contributions to sea-level rise, conditional on a specific LIG constraint:

$$p(f_{RCP} \mid y) = p(f_{RCP} \mid \theta_1, \theta_2) p(\theta_1, \theta_2 \mid y) \tag{4}$$

where $p(f_{RCP} \mid \theta_1, \theta_2)$ is the prior distribution of RCP8.5 emulator constructed above, and $p(\theta_1, \theta_2 \mid y)$ is the posterior probability of each parameter set conditioned on a specified LIG constraint. This probability can be decomposed using Bayes' theorem,

$$p(\theta_1, \theta_2 \mid y) \propto p(y \mid \theta_1, \theta_2) p(\theta_1, \theta_2) \tag{5}$$

where $p(\theta_1, \theta_2)$ is the uniform prior on the parameter space. Incorporating information about the true (unknown) LIG peak AIS mass loss, $g$,

$$p(y \mid \theta_1, \theta_2) \propto p(y \mid g) p(g \mid \theta_1, \theta_2) \tag{6}$$

where $p(g \mid \theta_1, \theta_2)$ is the emulator prior estimate of LIG sea-level contributions given the trained hyperparameters, and $p(y \mid g)$ is the probability distribution of the specified constraint given the unknown LIG peak AIS sea-level contributions. Here $p(y \mid g) \propto p(g \mid y)$ because $p(y)$, the prior probability of the LIG constraint, is taken to be uninformative. Substituting Eqn. 5 and 6 into Eqn. 4 we recover

$$p(f_{RCP} \mid y) \propto p(f_{RCP} \mid \theta_1, \theta_2) p(g \mid y) p(g \mid \theta_1, \theta_2) p(\theta_1, \theta_2) \tag{7}$$

which implies that the choice of prior and specification of a representative LIG constraint distribution, $p(g \mid y)$, both influence posterior projections of future AIS contributions to sea-level rise.

We demonstrate the utility of this approach in two ways. First, we show the result when the LIG contribution is assumed to be precisely known (to within a small range of 10 cm). The associated RCP8.5 distributions, conditional on the value of the LIG contributions, fully describe the efficacy of the LIG for constraining future sea-level contributions from Antarctica (given our model and prior). Second, we examine the posterior RCP8.5 distributions as a function of several specific LIG constraint distributions drawn from or adapted from the literature.

### 2.4 LIG Constraint Distributions

We prescribe a set of LIG constraint distributions, $p(g \mid y)$, to determine the associated posterior probability distributions of future Antarctic contributions to sea-level rise. Differences between these constraints are illustrative of the existing deep uncertainty in LIG Antarctic contributions. The density of each distribution (along with the LIG emulator prior distribution) is shown in Figure 4a.

*DeConto et al. (2019) uniform distribution* (**D19-U**): In contrast to the uniform distribution used to calibrate the ice-sheet model in DeConto and Pollard (2016) (cf. E19-U constraint below), the uniform constraint in DeConto et al. (2019) is narrower, given by $U(3.1\text{m}, 6.1\text{m})$. The constraint represents the peak extent of AIS retreat during the LIG. It is derived by assuming a total LIG global mean sea level in the early-LIG (∼130ka) of 4-7.5 m (Dutton, Carlson, et al., 2015; Dutton, Webster, et al., 2015), a small Greenland ice-sheet contribution in the early-LIG (1 m, Goelzer et al., 2016; Dahl-Jensen et al., 2013; Helsen et al., 2013), and a thermosteric rise of 0.4 m (McKay et al., 2011); mountain glacier contributions are ignored.

*DeConto et al. (2019) normal distribution* (**D19-N**): Whereas the uniform distribution assumes fixed limits on the LIG constraint but equal probabilities of LIG contributions between the limits, it is practical to explore the implications of the distribution's central value being more likely than the bounds. We therefore replace the uniform

distribution from DeConto et al. (2019) with a Gaussian distribution—taking the central value as the mean and the bounds as representing 2 standard deviations from the mean—to develop a constraint distribution that follows $\mathcal{N}(4.6\text{m}, (0.75\text{m})^2)$.

*DeConto et al. (2019) uniform distribution with a 33% reduction* (**D19-33% Red.**): A 33% reduction in the range of the uniform distribution is proposed in DeConto et al. (2019) as a hypothetical example of how estimates could improve with more precise paleoclimate constraints. The distribution is given by $U(3.6\text{m}, 5.6\text{m})$. This is only an example and does not represent any published distribution. Although bounds are equally reduced on either side of the distribution, that does not imply that posterior projections for future sea-level contributions will be equally affected in each tail (as we show, sections 3-4).

*Edwards et al. (2019) uniform distribution* (**E19-U**): The uniform distribution used to constrain the LIG Antarctic contributions in Edwards et al. (2019) is similar to the calibration of DeConto and Pollard (2016), and is given by $U(3.5\text{m}, 7.4\text{m})$. It is derived similarly to D19-U, except that the baseline peak sea-level budget terms are assumed to have broader uncertainties.

*Kopp et al. (2009) time slice at 125 ka* (**K09-125ka**): A probability distribution of AIS contributions to sea-level rise was compiled by Kopp et al. (2009)—and extended by Kopp et al. (2013)—using a statistical method combining a comprehensive database of proxy observations of LIG sea levels, an age model, and Gaussian process regression. Posterior probability distributions of AIS LIG sea levels were estimated over time by conditioning on local sea level and age measurements. To generate a simple LIG constraint from these distributions, we take a time slice at 125 ka. This approach is an overly simplified interpretation of the link between the ice-sheet emulator and the posterior LIG AIS distributions, because it assumes that the peak LIG contributions emulated by the ice-sheet model are representative of the synthesized observational record precisely at 125 ka.

*Kopp et al. (2009) maximum Antarctic contributions during the LIG* (**K09-Max-3kyrSmooth**): To make a more nuanced link between the ice-sheet model simulations and Kopp et al. (2009) constraints, we generate 2500 samples from the posterior probability distribution of mean global sea level conditioned upon sea-level observations and sampled ages from Kopp et al. (2009). This represents an approximate distribution of the global mean sea level maximum from the model in Kopp et al. (2009). Each sample is a realization of the evolution of AIS sea-level contributions during the LIG (between 129-114 ka). Because these samples can be noisy in time, we smooth each sample with a 3 kyr-window boxcar filter (other smoothing windows were explored, but here we focus on 3 kyr for brevity). The constraint distribution is then constructed from the peak (global maximum) Antarctic sea-level contribution of each smoothed sample (assuming each is equally likely), so that it shares an interpretation with the ice-sheet emulator (section 2.1).

For each LIG constraint distribution, we determine the associated posteriors of the parameter sets and future sea-level contribution projections following Eqn. 5 and 7.

This set of constraints is not intended to be exhaustive, but rather illustrative of range of current LIG constraints and their usefulness for informing future projections of Antarctic contributions to GMSL rise. Given the deep uncertainty in LIG sea levels, other constraint distributions could be justifiable. The methodology described here is flexible, so that any specified constraint may be assessed. In fact, the distributions in Figure 4b may be integrated over any specified range and weighting to directly determine RCP8.5 projections conditional on the LIG (section 3). However, any constraint distribution broader than the LIG emulator prior will not inform the posteriors of model parameters or future projections (section 3.2).

# 3 Results

## 3.1 Conditional Distributions

The posterior probability densities of RCP8.5 projections in 2100 conditioned on LIG Antarctic contributions to sea level are shown in Figure 4b. Along each bin of LIG contributions in Fig. 4b, the RCP8.5 probability densities are normalized to 1.0; densities are contoured on a log-scale. Conditioned projections in 2150 (shown in Supporting Information Figure S4) have a similar structure to Fig. 4b. For interpretation and comparison with the ice-sheet model parameter space, the posterior densities of CREVLIQ and CLIFVMAX conditioned on LIG contributions are shown in Figure 5. Fig. 4b is the primary result of this study, presenting a novel exploration and summary of the last interglacial's efficacy for informing future projections of sea-level rise.

Peak LIG contributions are relatively more informative on the extreme margins of the prior distribution (black curve, Fig. 4a). In these regions, there are fewer combinations of ice-sheet model parameter values that produce these sea levels than in the interior of the prior. These constraints on the margins are therefore also associated with narrower posteriors in future projections. For instance, if the LIG contributions were known to be ∼3.5 m (to within 10 cm), the median and associated 95% credible interval of RCP8.5 projections in 2100 are 7 cm and 4-15 cm, respectively. Likewise, if the LIG contributions were known to be higher, ∼6 m, the median and 95% credible intervals of 2100 projections are 81 cm and 68-95 cm. The latter range is partially an artifact of the ensemble prior: our restrictive prior limits the set of model parameter which can lead LIG contributions >6 m. In contrast, the narrow posteriors associated with the lower margin of the LIG prior are physically meaningful: they are associated with emulated ice-sheet model runs which have little or no retreat from MICI, i.e. CLIFVMAX<<1 $\frac{km}{yr}$ (Fig. 5).

The posteriors of RCP8.5 projections in 2100 associated with the interior of the prior LIG contributions are more broad than at the margins. Even if the LIG were known to within 10 cm in the prior's interior, it would be a less effective constraint on future projections. When the LIG contribution is 4.2 m, for instance, the associated 95% credible interval is 15-65 cm under RCP8.5 in 2100. This broad range results from the contrasting sensitivities of the LIG and RCP8.5 to parameter configurations (Supporting Information Figure S1). The LIG peak response exhibits multi-modal behavior indicating that different sectors of the ice sheet have been completely lost; the total losses of these runs are then insensitive to further small increases in parameter values. This result is shown in the coherent regions of parameter space which have similar sea level contributions and weak gradients in Fig. 2a. Comparing with Fig. 5a, there is a wide CLIFVMAX range which results in prior LIG contributions between 4 and 6 m. But transient RCP8.5 mass losses are strongly sensitive to the CLIFVMAX value when CREVLIQ>15 $\frac{m}{(myr^{-1})^2}$ (Fig. 2), and accordingly exhibit large ranges in future projections over this CLIFVMAX range. LIG contributions scale more linearly with CREVLIQ values until CREVLIQ>105 $\frac{m}{(myr^{-1})^2}$, and then LIG contributions are associated with broader ranges of CREVLIQ over 105-195 $\frac{m}{(myr^{-1})^2}$ (Fig. 5b).

These varying responses to model parameter configurations most clearly affects RCP8.5 projections when the median in 2100 *drops* from 63 to 32 cm as LIG contributions *increase* from 4.6 to 4.8 m. This non-intuitive result suggests that in some regions of parameter space, peak LIG contributions are influenced by different physical processes and parameters than transient RCP8.5 losses.

Fig. 4b and Fig. 5 may be used to explore any specified constraint distribution, by integrating the densities across the constraint with specified weightings. If, for instance, a field measurement showed that LIG AIS contributions were > 5 m, then the associated projected 2100 contributions under RCP8.5 would be ≥ 20 cm, with a median of

65 cm, and an upper bound of 1 m. Furthermore, the associated representative CREVLIQ and CLIFVMAX parameter values would be >90 $\frac{m}{(myr^{-1})^2}$ and >1 $\frac{km}{yr}$, respectively.

These conditional distributions are a powerful and novel tool for illustrating the links between ice-sheet model projections and observational records of the last interglacial. We illustrate and discuss how they may be used in the context of observational estimates in section 4.

### 3.2 Future Projections Given Specific LIG Constraint Distributions

The posterior probability distributions of sea-level contributions in 2100 and 2150 conditional on each LIG constraint are shown in Figure 6, along with the prior and histograms of the training simulations. Distributions are produced with kernel density estimation assuming a Silverman bandwidth (Silverman, 1986) reduced by 80% to prevent over-smoothing. Distribution quantiles are presented in Table 1. For reference, the posteriors of CREVLIQ/CLIFVMAX parameter sets associated with each specific constraint distribution are shown in Supporting Information Figure S5.

**Table 1.** Quantiles of projected Antarctic ice-sheet contributions in sea-level equivalent (m) in 2100 and 2150; each emulated distribution other than the prior is constrained using a specified last interglacial estimate distribution.

| **2100** Quantiles | Prior | D19-U | D19-N | D19-33% Red. | E19 | K09-125ka | K09-Max-3kyrSmooth |
|---|---|---|---|---|---|---|---|
| 5 | 0.07 | 0.07 | 0.07 | 0.08 | 0.07 | 0.07 | 0.09 |
| 25 | 0.20 | 0.20 | 0.23 | 0.22 | 0.23 | 0.21 | 0.31 |
| 50 | 0.42 | 0.40 | 0.40 | 0.38 | 0.44 | 0.43 | 0.52 |
| 75 | 0.64 | 0.61 | 0.58 | 0.54 | 0.65 | 0.64 | 0.72 |
| 95 | 0.85 | 0.83 | 0.78 | 0.69 | 0.85 | 0.85 | 0.88 |
| **2150** Quantiles | Prior | D19-U | D19-N | D19-33% Red. | E19 | K09-125ka | K09-Max-3kyrSmooth |
| 5 | 0.44 | 0.44 | 0.51 | 0.57 | 0.52 | 0.46 | 0.63 |
| 25 | 1.21 | 1.17 | 1.23 | 1.24 | 1.30 | 1.24 | 1.63 |
| 50 | 2.31 | 2.21 | 2.18 | 2.10 | 2.39 | 2.32 | 2.81 |
| 75 | 3.54 | 3.38 | 3.22 | 2.98 | 3.58 | 3.53 | 3.88 |
| 95 | 4.65 | 4.56 | 4.38 | 4.04 | 4.66 | 4.64 | 4.79 |

Through 2100, specific LIG constraints from previous studies are not very effective at narrowing uncertainties in future projections. Quantiles of the prior, D19-U, E19-U, and K09-125ka are all within 5 cm of one another across their future projection distributions (Table 1). D19-N weights the distribution towards the lower end of projections, lowering the $95^{th}$ percentile (relative to the prior) by 7 cm. The hypothetical D19-33% Red. distribution is more influential on the projected distributions in 2100, reducing the $95^{th}$ percentile by 16 cm and slightly decreasing the median projection by 4 cm. The K09-Max-3kyrSmooth distribution re-weights the projection distribution towards the upper tail (cf. Fig. 4a), raising the median and $75^{th}$ percentiles by 8-10 cm.

CREVLIQ/CLIFVMAX posteriors (Fig. S5) show that there is no set of parameter values which are consistently unlikely across the range of LIG constraints. Thus, deductions about the viability of regions of the parameter space will depend entirely on the specific LIG constraint applied. For instance, if we consider only the E19-U constraint,

we find the least likely parameter sets are when CLIFVMAX << 1 (Figure S5d). This result implies that MICI is necessary for emulated LIG values to meet the E19-U criterion, in contrast to the conclusions of Edwards et al. (2019). The differences between this study and Edwards et al. (2019) are the ensemble structure, as well as enhanced model physics and a reduced ocean bias correction in our training runs (section 2.1). Overall, none of the existing LIG constraints are able to exclude MICI as a primary loss mechanism, which would require LIG AIS contributions <3 m.

Comparisons between the prior and specific constraint distributions (Fig. 4a) reveal a challenge in using the LIG to constrain future projections of future sea-level rise. The training simulation prior nearly coincides with (or is more narrow than) the existing LIG constraint distributions. Whereas this indicates that the ice-sheet model is able to faithfully reproduce peak LIG AIS mass losses, it also implies that current LIG estimates are not strong constraints on model parameter likelihoods and projection posteriors. A larger initial distribution of simulation parameters and parameter values is necessary to methodically and holistically constrain the ice-sheet model behavior and associated future projections.

LIG constraints with narrow ranges tend to influence the upper-tail probabilities of future projections more than the lower-tail probabilities, which provides insight into the physical connections between LIG estimates and future mass loss outcomes. The mode of the prior distribution centered at 6 m (Fig 4a) is associated with the parameter region where CREVLIQ > 105 and CLIFVMAX > 7 (Fig. 2 and S5). When a LIG constraint weights this region's emulated members as less likely (or given no weight in the case of D19-33% Red.), the upper-tail probability of future projections is reduced. In contrast, although the D19-33% Red. distribution affects the lower tail of the LIG contributions (Fig. 4a) and reduces the probabilities of parameter sets where CLIFVMAX << 1 (Figure S5c), the extent to which it constrains the lower tail of future sea-level contributions in 2100 is limited. There is still density in lower end of the LIG prior which has not been constrained, primarily where CLIFVMAX > 1, CREVLIQ < 30, so the lower tail of future projection distribution in 2100 is largely unaffected. To raise the $5^{th}$ quantile of 2100 projections by 10 cm (to 17 cm), the lower bound of a uniform LIG constraint distribution would have to exceed 4.5 m (cf. Fig. 4b), or non-uniform weightings of the LIG constraint distribution would need to heavily weight toward values at the upper end of the LIG prior.

Because emulator future projections of AIS mass loss are driven by instabilities (MISI and MICI), the prior distribution of future loss is positively skewed over time (Fig. 1 and 6). As shown recently by Robel et al. (2019), instabilities on a reverse-sloping bed drive a greater rate of mass loss among emulator samples which have retreated more than the rate among samples which have retreated less; this results in a positively skewed distribution of AIS contributions to sea level. Furthermore, because LIG constraints distributions restrict the most unstable regions of model parameter space, LIG constraints become increasingly informative on future sea-level contributions with time. We illustrate this by plotting the timeseries of quantile differences between D19-33% Red. and the prior future mass losses (Figure 7); the D19-33% Red. LIG constraint substantially reduces the magnitude of the $95^{th}$ quantile over time, whereas the lower quantiles are less affected. This result can also be seen by visually comparing the 2150 projection distributions with those in 2100 (Fig. 6 and numerically in Table 1). We conclude that even if observation-based LIG constraints are of little utility for reducing sea-level projection uncertainties in the near-term, they could become more meaningful over time as they restrict the most unstable projections.

## 4 Discussion

Conditional posterior distributions (Fig. 4b-5) show how LIG estimates influence future sea-level rise projections. They also suggest which physical processes are most likely linked to paleoclimate ice-sheet mass loss. Concurrently, any improvements in understanding physical processes in the ice-sheet will also indicate which LIG contributions are most likely. Whereas there would still be uncertainty even if the LIG AIS contributions were known precisely, the LIG still has the potential to be a useful constraint on AIS sea level contributions in a warming world (cf. Fischer et al., 2018). A main benefit of our study is that its results may inform future research and observational efforts to understand LIG sea levels.

Determining sea levels during the LIG period and closing the LIG peak sea level budget are challenging problems. Field observations have large uncertainties, related to measurement error or confounding processes such glacial isostatic adjustment (GIA) or mantle dynamic topography (DT), which makes it difficult to reconstruct LIG sea levels (Rovere et al., 2016; Hibbert et al., 2016; Capron et al., 2019). The LIG may have exhibited variability with multiple global sea-level peaks (Kopp, Dutton, & Carlson, 2017), indicating short-term fluctuations (e.g., Rohling et al., 2008), or distinct out-of-phase mass losses of the Greenland and Antarctic ice sheets (Dutton, Carlson, et al., 2015); this variability, however, is still under debate (Barlow et al., 2018). Lacking much near-field evidence, the AIS is typically invoked as an uncertain residual contributor. Yet LIG estimates of the Greenland's contributions to GMSL also have deep uncertainties, so it is difficult to disentangle the relative roles of these two ice sheets (Dutton, Carlson, et al., 2015, their Figure 3).

Our method is able to show how these uncertainties in proxy-based reconstructions of LIG sea levels reflect on uncertainties in future AIS melting. To illustrate this, we calculate the range of 95% credible interval of AIS sea-level contributions under RCP8.5 in 2100, varying the LIG AIS uncertainty range according to three different scenarios for GMSL. Scenarios are derived from a milestone study by Dutton, Webster, et al. (2015), who used sea level proxies in the Seychelles to constrain polar ice sheets melting in the LIG. We note that this is a close-to-ideal case study, because GIA and DT predictions in the Seychelles have relatively small uncertainties. All uncertainties are $1\sigma$ and assumed to follow a normal distribution. The scenarios are:

1. Relative sea level coinciding with the highest in situ coral measured by Dutton, Webster, et al. (2015) with high-accuracy surveying techniques. The coral assemblage is interpreted as "likely intertidal" and its elevation is 8±0.2 m above modern sea level.
2. While scenario 1 is illustrative of very small uncertainties in LIG sea level estimates, it is also incomplete because it does not account for departures from eustasy due to GIA and sea level fingerprints. These were calculated by Dutton, Webster, et al. (2015) using model results from Dutton and Lambeck (2012) and Hay et al. (2014). Using these estimates, Dutton, Webster, et al. (2015) calculated that LIG GMSL rise was 7.6±1.7 m.
3. Austermann et al. (2017) showed that mantle dynamic topography and ocean subsidence effects must be corrected before GMSL can be calculated from field data. In their study they remark that DT corrections are subject to large uncertainties that must be further investigated; here we use their model results for the Seychelles to illustrate how accounting for DT and ocean subsidence influences paleo GMSL estimates and their uncertainties. Subtracting ocean subsidence (-1.4 m) and DT as modelled in Austermann et al. (2017) (-0.8±1.8m) from scenario 2, we calculate that LIG GMSL rise was 9.2±2.5 m.

For each of these three scenarios, we calculate LIG AIS sea-level contributions by subtracting the contributions of the Greenland Ice Sheet (GrIS), mountain glaciers and thermosteric expansion (TMG) following the budgetary approach of Dutton, Carlson, et al. (2015). First, we assume that the contributions of GrIS and TMG to LIG sea level are known (2 m and 1 m, respectively), with no error. We compare with the assumption that, instead, GrIS contributed 2 m$\pm$1.5 m to LIG GMSL, as shown in Dutton, Carlson, et al. (2015, Figure 3). We set the contributions from mountain glaciers and thermosteric expansion to 1 m (Dutton, Carlson, et al., 2015), with arbitrary uncertainties of $\pm$0.2 m.

This exercise (Figure 8A-C) shows that, regardless of the amount of LIG AIS melting, the LIG can only substantially reduce uncertainties in future AIS melting if the following two conditions are met: 1) sea level data and departures from eustasy are known with $\pm 1\sigma$ uncertainties of a few decimeters and 2) GrIS and TMG uncertainties are small ($<$1 m). This could be considered a discouraging message for the paleo communities working on these topics, i.e. the large intrinsic uncertainties that characterize GrIS and proxy-based ESL estimates may seem insurmountable. But instead we point out that this knowledge gap provides a unique opportunity to do innovative, timely and important research that feeds directly into the open research questions in the paleo sea level and ice sheet communities (Capron et al., 2019).

Results further suggest that the storyline of LIG sea level evolution has a strong influence on whether the LIG is able to constrain future sea level changes. Greenland and Antarctic sea-level contributions are inextricably linked during the LIG: knowledge or evidence about one will inform the other. We illustrate this in Figure 8D, showing that if LIG total GMSL estimates were more precise (errors of $\pm$0.5 m), then the mean GrIS contributions would strongly reflect on future AIS contributions to sea-level rise. By fixing the GMSL estimates (including TMG) at 7.5 m and varying the mean estimate for GrIS, we find future AIS mass loss distributions which span from very low estimates (when GrIS contributions are high, and thus LIG AIS contributions are inferred to be low) to broadly uncertain or high future loss estimates (when GrIS contributions are low, and LIG AIS contributions are accordingly high). This links between the ice sheets implies that 1) efforts to improve estimates of GrIS can directly inform future AIS sea level projections, and that 2) the timing of LIG GrIS loss compared with LIG AIS loss is pivotal (Kopp, Dutton, & Carlson, 2017).

There is some evidence that the GrIS was partially persistent during the LIG, contributing only $\sim$2 m (Colville et al., 2011). But it is difficult to establish precise chronologies (Dutton, Carlson, et al., 2015). A storyline in which GrIS and AIS mass losses peak simultaneously has a very different interpretation from one in which they peak several thousand years apart, each implying different AIS projected contributions to future sea-level rise. Furthermore, the links between LIG AIS and physical ice-loss mechanisms (section 3) implies that these physical processes and LIG estimates are interwoven; epistemic advances in any one of these areas will inform the others.

The mismatch between between transient future ice-sheet losses and peak LIG losses limits the effectiveness of the LIG as a constraint. Historically, studies of the LIG have focused primarily on gathering geological evidence of peak LIG GMSL, in part because these are less challenging measurements to make in the field. But a comparison of modeled LIG and future timeseries in Fig. 1 shows that the transient *onset* period of LIG losses closely mirrors future losses, with similar dependencies on model physics and parameters. Therefore, quality estimates of the LIG onset period are highly desirable for constraining AIS changes and future sea-level rise. To this point, sampling biases and the requirement for precise chronologies have thwarted these efforts; we propose that further efforts be made to improve estimates of the LIG onset. These could be particularly useful for calibrating ice-sheet model parameters and informing future projections of sea-level rise. As a coherent picture of LIG sea levels emerges, combining LIG constraints

with probabilistic distributions from ice-sheet models—as this study has done—will improve the precision of future sea level projections.

## 5 Summary and Conclusions

This study has emulated an ice-sheet model to investigate whether last interglacial (LIG) Antarctic mass loss estimates are able to constrain projections of future sea-level rise under a high-emissions scenario. Ice-sheet model ensembles were developed with runs spanning over a broader range of parameter values than previously explored (DeConto & Pollard, 2016). Using a Bayesian updating approach, emulated projections of future sea-level rise were conditioned on peak LIG contributions to investigate how future mass loss distributions depend on LIG estimates. A set of previously proposed specific LIG constraint distributions (several of which have been used to calibrate ice-sheet model projections) were also employed to explore their effectiveness for constraining future sea-level rise. Emulated LIG distributions were combined with field measurement scenarios (and their uncertainties) to illustrate how improvements in LIG observational estimates could potentially narrow uncertainties in future Antarctic ice sheet projections.

Results explicitly show how estimated LIG Antarctic contributions are able to inform which ice-sheet model parameter values are most likely, which in turn inform future projections of sea-level rise. However, LIG Antarctic contributions have deep uncertainty (e.g., Düsterhus et al., 2016), and not all specific LIG estimates inform future projections equally. For instance, if LIG contributions were known to be <4 m, then marine ice-cliff instability (MICI) is very unlikely to be a primary loss mechanism in future Antarctic mass loss. Likewise, if LIG contributions were known to be >6 m, they would imply substantial future mass losses associated with MICI. In either case, uncertainties in future projections would narrow considerably, but some uncertainty would remain because peak LIG Antarctic mass losses have somewhat different sensitivities to ice-sheet model parameters than future changes do (i.e. the peak LIG is an imperfect analog for future sea level rise). LIG observations which inform the upper and lower limits of the modeled prior distribution would be valuable for improving future projections (in the context of this specific model and ensemble). Because ice-sheet model parameter likelihoods and LIG sea level estimates are closely linked, evidence of constraints on one informs the other. For instance, if there are indications that MICI is not a viable loss mechanism, results here indicate that LIG Antarctic sea-level contributions were very likely <4 m at their peak.

Peak LIG constraints which have been previously used to calibrate ice-sheet model projections (e.g., DeConto & Pollard, 2016; Edwards et al., 2019) are inadequate to restrict a wide range of model parameter values. Consequently, this study cannot exclude the possibility of MICI as a driver of Antarctic ice-sheet retreat on the basis of the best available estimates of peak LIG Antarctic sea-level contributions.

Recently proposed constraints on peak LIG Antarctic contributions to sea levels (DeConto et al., 2019) of between 3.1 and 6.1 m—based on assuming residual Antarctic contributions in a sea-level budget analysis (Dutton, Carlson, et al., 2015)—restrict the regions of model parameter space with the most unstable solutions. These unstable solutions lose mass more quickly over time than their more stable counterparts. Accordingly, their exclusion (through Bayesian updating, conditioning on the LIG) results in a posterior distribution of future projections which is less positively skewed over time (cf. Robel et al., 2019). The LIG constraint therefore becomes more influential on sea-level contribution projections with time, through at least 2150. Consequently, a LIG constraint which may not be useful in the near-term could still be important for informing projections on longer time scales.

Conditioning future AIS mass losses on peak LIG sea level exposes the direct links between paleo sea level reconstructions and future sea-level rise. Improvements in field measurements, reductions in uncertainties from glacial isostatic adjustment or dynamic topography, and better chronologies of Antarctic and Greenland ice-sheet retreat during the LIG could all reduce uncertainties in future projections. These results provide strong motivation and support for continued collaborations between the paleo sea level and ice-sheet communities.

Past studies of LIG sea level have focused primarily on peak global mean sea levels, as they are more readily and reliably measurable, and because it is difficult to establish accurate and precise sea-level chronologies (Dutton, Carlson, et al., 2015). But peak LIG Antarctic ice-sheet mass losses are not necessarily representative of the transient changes the Antarctic ice-sheet may experience in the coming decades and centuries. This mismatch between the future and the past limits the applicability of LIG constraints on future Antarctic mass loss. Even if LIG Antarctic contributions were known to within 10 cm, there would still be decimeter-scale uncertainties in projections of future Antarctic contributions to sea-level rise. Results herein suggest that estimates of global mean sea levels during the LIG onset would likely provide more appropriate constraints on future projections. Additional field observations and studies detailing or inferring Antarctic changes during the LIG onset are needed.

Although the ice-sheet model ensemble used herein improves on that of DeConto and Pollard (2016), the associated emulator prior distribution and LIG constraint distributions are very similar. This implies that the simulated ensemble members comprise a prior distribution which is too narrowly constructed, and which should be expanded in future studies. Despite this inherent drawback, this study's methodology remains useful for illustrating the current limitations of LIG constraints, and has utility in guiding promising avenues of future observational research. Constructing a larger prior (over more parameters values and more unique parameters) is only feasible with advanced computational approaches and a reduced model resolution (which may not properly represent complex ice-sheet processes or instabilities Seiyon Lee et al., 2019). Ultimately, an approach blending a larger prior and the methodologies herein will be needed for future holistic explorations of LIG constraints.

The LIG is an imperfect analog for ice-sheet sensitivities to climate warming and for future sea-level rise (e.g., Capron et al., 2019, and references therein). Uncertainties in ice-sheet physics and observational evidence currently limit the LIG's effectiveness for informing future sea levels. Despite these limitations, this study has specifically illustrated how models (and emulation) may be useful for interpreting and guiding paleo sea level observational constraints. A major ongoing research objective is to continue strategically gathering field observations, in order to improve understanding and estimates of LIG sea levels. Such improvements, along with continued integration with modeling and statistical methods, will increase confidence in the physics and projections of Antarctic contributions to sea-level rise over the coming centuries.

**Acknowledgments**

We thank Andrea Dutton and Anna Ruth Halberstadt for helpful comments which improved this manuscript. DG, RK, RD, and DP were supported by NSF Grant ICER-1663807 and NASA Grant 80NSSC17K0698. EA and RK were supported by NSF Grant OCE-1702587. This paper grew, in part, out of discussions at the 2018 PALeo constraints on SEA level rise (PALSEA) annual meeting (see Capron et al., 2019). Model simulations used in this study are freely available at `https://doi.org/10.5281/zenodo.3478486`. Code to perform these analyses will be available upon publication. GP regression was performed with GPflow (Matthews et al., 2017); some colormaps provided by Crameri (2018).

## References


Arthern, R. J., & Williams, C. R. (2017). The sensitivity of West Antarctica to the submarine melting feedback. *Geophysical Research Letters*, *44*(5), 2352–2359. doi: 10.1002/2017GL072514

Ashe, E. L., Cahill, N., Hay, C., Khan, N. S., Kemp, A., Engelhart, S. E., ... Kopp, R. E. (2019). Statistical modeling of rates and trends in holocene relative sea level. *Quaternary Science Reviews*, *204*, 58 - 77. Retrieved from `http://www.sciencedirect.com/science/article/pii/S0277379118302130` doi: https://doi.org/10.1016/j.quascirev.2018.10.032

Austermann, J., Mitrovica, J. X., Huybers, P., & Rovere, A. (2017). Detection of a dynamic topography signal in last interglacial sea level records. *Geophysical Research Abstracts EGU General Assembly*, *19*(July), 2017–13646. Retrieved from `https://meetingorganizer.copernicus.org/EGU2017/EGU2017-13646.pdf` doi: 10.1126/sciadv.1700457

Bakker, A. M., Louchard, D., & Keller, K. (2017). Sources and implications of deep uncertainties surrounding sea-level projections. *Climatic Change*, *140*(3-4), 339–347. Retrieved from `http://dx.doi.org/10.1007/s10584-016-1864-1` doi: 10.1007/s10584-016-1864-1

Bakker, A. M., Wong, T. E., Ruckert, K. L., & Keller, K. (2017). Sea-level projections representing the deeply uncertain contribution of the West Antarctic ice sheet. *Scientific Reports*, *7*(1), 1–7. doi: 10.1038/s41598-017-04134-5

Bamber, J. J. L., Oppenheimer, M., Kopp, R. E., Aspinall, W. P., & Cooke, R. M. (2019). Ice sheet contributions to future sea-level rise from structured expert judgement. *Proceedings of the National Academy of Sciences*, *in review*, 1–6. doi: 10.1073/pnas.1817205116

Barlow, N. L., McClymont, E. L., Whitehouse, P. L., Stokes, C. R., Jamieson, S. S., Woodroffe, S. A., ... Sanchez-Montes, M. L. (2018). Lack of evidence for a substantial sea-level fluctuation within the Last Interglacial. *Nature Geoscience*, *11*(9), 627–634. Retrieved from `http://dx.doi.org/10.1038/s41561-018-0195-4` doi: 10.1038/s41561-018-0195-4

Bassis, J. N., & Walker, C. C. (2012). Upper and lower limits on the stability of calving glaciers from the yield strength envelope of ice. *Proceedings of the Royal Society A: Mathematical, Physical and Engineering Sciences*, *468*(2140), 913–931. doi: 10.1098/rspa.2011.0422

Bastos, L. S., & O'Hagan, A. (2009). Diagnostics for gaussian process emulators. *Technometrics*, *51*(4), 425–438. doi: 10.1198/TECH.2009.08019

Buchanan, M. K., Kopp, R. E., Oppenheimer, M., & Tebaldi, C. (2016). Allowances for evolving coastal flood risk under uncertain local sea-level rise. *Climatic Change*, *137*(3-4), 347–362. Retrieved from `http://dx.doi.org/10.1007/s10584-016-1664-7` doi: 10.1007/s10584-016-1664-7

Buchanan, M. K., Oppenheimer, M., & Kopp, R. E. (2017). Amplification of flood frequencies with local sea level rise and emerging flood regimes. *Environmental Research Letters*, *12*(6). doi: 10.1088/1748-9326/aa6cb3

Bulthuis, K., Arnst, M., Sun, S., & Pattyn, F. (2019). *Uncertainty quantification of the multi-centennial response of the Antarctic Ice Sheet to climate change*. doi: 10.5194/tc-2018-220

Capron, E., Govin, A., Feng, R., Otto-Bliesner, B. L., & Wolff, E. W. (2017). Critical evaluation of climate syntheses to benchmark CMIP6/PMIP4 127 ka Last Interglacial simulations in the high-latitude regions. *Quaternary Science Reviews*, *168*, 137–150. Retrieved from `https://doi.org/10.1016/j.quascirev.2017.04.019` doi: 10.1016/j.quascirev.2017.04.019

Capron, E., Govin, A., Stone, E. J., Masson-Delmotte, V., Mulitza, S., Otto-Bliesner, B., ... Wolff, E. W. (2014). Temporal and spatial structure of multi-millennial temperature changes at high latitudes during the Last interglacial. *Quaternary Science Reviews*, *103*, 116–133. doi: 10.1016/

j.quascirev.2014.08.018

Capron, E., Rovere, A., Austermann, J., Axford, Y., Barlow, N. L., Carlson, A. E., ... Wolff, E. W. (2019). *Challenges and research priorities to understand interactions between climate, ice sheets and global mean sea level during past interglacials.* Retrieved from https://linkinghub.elsevier.com/retrieve/pii/S0277379119305207 doi: 10.1016/j.quascirev.2019.06.030

Colville, E., Carlson, A., Beard, B., Hatfield, R., Stoner, J., Reyes, A., & Ullman, D. (2011, 07). Sr-nd-pb isotope evidence for ice-sheet presence on southern greenland during the last interglacial. *Science (New York, N.Y.)*, *333*, 620-3. doi: 10.1126/science.1204673

Crameri, F. (2018). Geodynamic diagnostics, scientific visualisation and staglab 3.0. *Geoscientific Model Development*, *11*(6), 2541–2562. Retrieved from https://www.geosci-model-dev.net/11/2541/2018/ doi: 10.5194/gmd-11-2541-2018

Dahl-Jensen, D., Albert, M. R., Aldahan, A. A., Azuma, N., Balslev-Clausen, D., Baumgartner, M. R., ... Community, N. (2013). Eemian interglacial reconstructed from a greenland folded ice core. *Nature*, *493*, 489-494.

DeConto, R. M., & Pollard, D. (2016). Contribution of Antarctica to past and future sea-level rise. *Nature*, *531*(7596), 591–597. Retrieved from http://dx.doi.org/10.1038/nature17145 doi: 10.1038/nature17145

DeConto, R. M., Pollard, D., Alley, R. B., Velicogna, I., & Gasson, E. (2019). The Paris Climate Agreement and future sea level rise from Antarctica. *Nature Climate Change, under review*.

Düsterhus, A., Tamisiea, M. E., & Jevrejeva, S. (2016). Estimating the sea level highstand during the last interglacial: A probabilistic massive ensemble approach. *Geophysical Journal International*, *206*(2), 900–920. doi: 10.1093/gji/ggw174

Dutton, A., Carlson, A. E., Long, A. J., Milne, G. A., Clark, P. U., DeConto, R., ... Raymo, M. E. (2015). Sea-level rise due to polar ice-sheet mass loss during past warm periods. *Science*, *349*(6244). doi: 10.1126/science.aaa4019

Dutton, A., & Lambeck, K. (2012). Ice volume and sea level during the last interglacial. *Science*, *337*(6091), 216–219. doi: 10.1126/science.1205749

Dutton, A., Webster, J. M., Zwartz, D., Lambeck, K., & Wohlfarth, B. (2015). Tropical tales of polar ice: Evidence of Last Interglacial polar ice sheet retreat recorded by fossil reefs of the granitic Seychelles islands. *Quaternary Science Reviews*, *107*, 182e196–196. Retrieved from http://dx.doi.org/10.1016/j.quascirev.2014.10.025 doi: 10.1016/j.quascirev.2014.10.025

Edwards, T. L., Brandon, M., Durand, G., Edwards, N. R., Golledge, N. R., Holden, P. B., ... Ritz, C. (2019). Revisiting Antarctic ice loss due to marine ice cliff instability. *Nature*, 1–35. Retrieved from http://dx.doi.org/10.1038/s41586-019-0901-4 doi: 10.1038/s41586-019-0901-4

Favier, L., Durand, G., Cornford, S. L., Gudmundsson, G. H., Gagliardini, O., Gillet-Chaulet, F., ... Le Brocq, A. M. (2014). Retreat of Pine Island Glacier controlled by marine ice-sheet instability. *Nature Climate Change*, *4*(2), 117–121. Retrieved from http://dx.doi.org/10.1038/nclimate2094 doi: 10.1038/nclimate2094

Fischer, H., Meissner, K. J., Mix, A. C., Abram, N. J., Austermann, J., Brovkin, V., ... Sarnthein, M. (2018). Palaeoclimate constraints on the impact of 2 C anthropogenic warming and beyond. *Nature Geoscience*. doi: 10.1038/s41561-018-0146-0

Fuller, R. W., Wong, T. E., & Keller, K. (2017). Probabilistic inversion of expert assessments to inform projections about Antarctic ice sheet responses. , 6–9.

Gardner, A. S., Moholdt, G., Scambos, T., Fahnstock, M., Ligtenberg, S., Van Den Broeke, M., & Nilsson, J. (2018). Increased West Antarctic and unchanged East Antarctic ice discharge over the last 7 years. *Cryosphere*, *12*(2), 521–547.

doi: 10.5194/tc-12-521-2018

Goelzer, H., Huybrechts, P., Marie-France, L., & Fichefet, T. (2016). Last Interglacial climate and sea-level evolution from a coupled ice sheet-climate model. *Climate of the Past*, *12*(12), 2195–2213. doi: 10.5194/cp-12-2195-2016

Goelzer, H., Nowicki, S., Edwards, T., Beckley, M., Abe-Ouchi, A., Aschwanden, A., ... Ziemen, F. A. (2018). Design and results of the ice sheet model initialisation initMIP-Greenland: An ISMIP6 intercomparison. *Cryosphere*, *12*(4), 1433–1460. doi: 10.5194/tc-12-1433-2018

Golledge, N. R., Kowalewski, D. E., Naish, T. R., Levy, R. H., Fogwill, C. J., & Gasson, E. G. (2015). The multi-millennial Antarctic commitment to future sea-level rise. *Nature*, *526*(7573), 421–425. doi: 10.1038/nature15706

Hansen, J., Johnson, D., Lacis, A., Lebedeff, S., Lee, P., Rind, D., & Russell, G. (1981). Climate impact of increasing atmospheric carbon dioxide. *Science*, *213*(4511), 957–966. doi: 10.1126/science.213.4511.957

Hay, C., Mitrovica, J. X., Gomez, N., Creveling, J. R., Austermann, J., & Kopp, R. R. (2014). The sea-level fingerprints of ice-sheet collapse during interglacial periods. *Quaternary Science Reviews*, *87*, 60–69. Retrieved from `http://dx.doi.org/10.1016/j.quascirev.2013.12.022` doi: 10.1016/j.quascirev.2013.12.022

Helsen, M. M., van de Berg, W. J., van de Wal, R. S. W., van den Broeke, M. R., & Oerlemans, J. (2013). Coupled regional climatendash;ice-sheet simulation shows limited greenland ice loss during the eemian. *Climate of the Past*, *9*(4), 1773–1788. Retrieved from `https://www.clim-past.net/9/1773/2013/` doi: 10.5194/cp-9-1773-2013

Hibbert, F. D., Rohling, E. J., Dutton, A., Williams, F. H., Chutcharavan, P. M., Zhao, C., & Tamisiea, M. E. (2016). Coral indicators of past sea-level change: A global repository of U-series dated benchmarks. *Quaternary Science Reviews*, *145*, 1–56. Retrieved from `http://dx.doi.org/10.1016/j.quascirev.2016.04.019` doi: 10.1016/j.quascirev.2016.04.019

Horton, B. P., Kopp, R. E., Garner, A. J., Carling, C., Khan, N. S., Roy, K., & Shaw, T. A. (2018). Mapping sea-level change in time, space and probability. *Annual Reviews of Energy and the Environment*, *in review*(July), 1–41.

IMBIE-Team. (2018). Mass balance of the Antarctic ice sheet from 1992 to 2017. *Nature*, *558*, 219–222. doi: 10.1098/rsta.2006.1792

Joughin, I., Smith, B. E., & Medley, B. (2014). Marine ice sheet collapse potentially under way for the thwaites glacier basin, West Antarctica. *Science*, *344*(6185), 735–738. doi: 10.1126/science.1249055

Kennedy, M. C., & O'Hagan, A. (2001). Bayesian calibration of computer models. *Journal of the Royal Statistical Society: Series B (Statistical Methodology)*, *63*(3), 425–464. Retrieved from `http://doi.wiley.com/10.1111/1467-9868.00294` doi: 10.1111/1467-9868.00294

Kopp, R. E., DeConto, R. M., Bader, D. A., Hay, C. C., Horton, R. M., Kulp, S., ... Strauss, B. H. (2017). Evolving Understanding of Antarctic Ice-Sheet Physics and Ambiguity in Probabilistic Sea-Level Projections. *Earth's Future*, *5*(12), 1217–1233. doi: 10.1002/2017EF000663

Kopp, R. E., Dutton, A., & Carlson, A. (2017). Centennial- to millennial-scale sea-level change during the Holocene and Last Interglacial periods. *Past Global Changes Magazine*, *25*(3), 148–149. doi: 10.22498/pages.25.3.148

Kopp, R. E., Horton, R. M., Little, C. M., Mitrovica, J. X., Oppenheimer, M., Rasmussen, D. J., ... Tebaldi, C. (2014). Probabilistic 21st and 22nd century sea-level projections at a global network of tide-gauge sites. *Earth's Future*, *2*(8), 383–406. Retrieved from `http://doi.wiley.com/10.1002/2014EF000239` doi: 10.1002/2014EF000239

Kopp, R. E., Simons, F. J., Mitrovica, J. X., Maloof, A. C., & Oppenheimer, M. (2009). Probabilistic assessment of sea level during the last interglacial stage.

*Nature*, *462*(7275), 863–867. Retrieved from http://dx.doi.org/10.1038/nature08686 doi: 10.1038/nature08686

Kopp, R. E., Simons, F. J., Mitrovica, J. X., Maloof, A. C., & Oppenheimer, M. (2013). A probabilistic assessment of sea level variations within the last interglacial stage. *Geophysical Journal International*, *193*(2), 711–716. doi: 10.1093/gji/ggt029

Lempert, R. J., & Collins, M. T. (2007). Managing the risk of uncertain threshold responses: Comparison of robust, optimum, and precautionary approaches. *Risk Analysis*, *27*(4), 1009–1026. doi: 10.1111/j.1539-6924.2007.00940.x

Matthews, A. G. d. G., van der Wilk, M., Nickson, T., Fujii, K., Boukouvalas, A., Le'on-Villagr'a, P., ... Hensman, J. (2017, apr). GPflow: A Gaussian process library using TensorFlow. *Journal of Machine Learning Research*, *18*(40), 1-6. Retrieved from http://jmlr.org/papers/v18/16-537.html

McKay, N. P., Overpeck, J. T., & Otto-Bliesner, B. L. (2011). The role of ocean thermal expansion in Last Interglacial sea level rise. *Geophysical Research Letters*, *38*(14), 4–9. doi: 10.1029/2011GL048280

Meehl, G. a., Washington, W. M., & Collins, W. D. (2005). How Much More Global Warming and Sea Level How Much More Global Warming and Sea Level Rise ? *Science (New York, N.Y.)*, *307*(5716), 1769–1773. Retrieved from http://adsabs.harvard.edu/cgi-bin/nph-data{_}query?bibcode=2005Sci...307.1769M{\&}link{_}type=ABSTRACT{\%}5Cnpapers3://publication/doi/10.1126/science.1106663 doi: 10.1126/science.1106663

Mengel, M., Levermann, A., Frieler, K., Robinson, A., Marzeion, B., & Winkelmann, R. (2016). Future sea level rise constrained by observations and long-term commitment. *Proceedings of the National Academy of Sciences*, *113*(10), 2597–2602. Retrieved from http://www.pnas.org/lookup/doi/10.1073/pnas.1500515113 doi: 10.1073/pnas.1500515113

Mengel, M., Nauels, A., Rogelj, J., & Schleussner, C.-F. (2018). The sea level legacy of the Paris Agreement and the effect of delayed mitigation action. *Nature Communications*, 1–10. Retrieved from http://dx.doi.org/10.1038/s41467-018-02985-8 doi: 10.1038/s41467-018-02985-8

Mercer, J. H. (1968). Antarctic ice and Sangamon sea level. *International Association of Scientific Hydrology*, *79*(139), 217–225. Retrieved from https://iahs.info/uploads/dms/079020.pdf

Nowicki, S. M., Payne, A., Larour, E., Seroussi, H., Goelzer, H., Lipscomb, W., ... Shepherd, A. (2016). Ice Sheet Model Intercomparison Project (ISMIP6) contribution to CMIP6. *Geoscientific Model Development*, *9*(12), 4521–4545. doi: 10.5194/gmd-9-4521-2016

Oppenheimer, M., & Alley, R. B. (2016). How high will the seas rise? *Science*, *354*(6318), 1375–1377. doi: 10.1126/science.aak9460

Parizek, B. R., Christianson, K., Alley, R. B., Voytenko, D., Vaňková, I., Dixon, T. H., ... Holland, D. M. (2019). Ice-cliff failure via retrogressive slumping. *Geology*, *47*(5), 449–452. doi: 10.1130/G45880.1

Pollard, D., Chang, W., Haran, M., Applegate, P., & DeConto, R. (2016). Large ensemble modeling of the last deglacial retreat of the West Antarctic Ice Sheet: Comparison of simple and advanced statistical techniques. *Geoscientific Model Development*, *9*(5), 1697–1723. doi: 10.5194/gmd-9-1697-2016

Pollard, D., & DeConto, R. M. (2009). Modelling West Antarctic ice sheet growth and collapse through the past five million years. *Nature*, *458*(7236), 329–332. Retrieved from http://dx.doi.org/10.1038/nature07809 doi: 10.1038/nature07809

Pollard, D., & DeConto, R. M. (2012). Description of a hybrid ice sheet-shelf model, and application to Antarctica. *Geoscientific Model Development*, *5*(5), 1273–1295. doi: 10.5194/gmd-5-1273-2012

Pollard, D., DeConto, R. M., & Alley, R. B. (2015). Potential Antarctic Ice Sheet

retreat driven by hydrofracturing and ice cliff failure. *Earth and Planetary Science Letters*, *412*, 112–121. Retrieved from http://dx.doi.org/10.1016/j.epsl.2014.12.035 doi: 10.1016/j.epsl.2014.12.035

Pollard, D., Gomez, N., DeConto, R., & Han, H. K. (2018). Estimating Modern Elevations of Pliocene Shorelines Using a Coupled Ice Sheet-Earth-Sea Level Model. *Journal Geophysical Research: Earth Surface*, 1–13. doi: 10.1029/2018JF004745

Pollard, D., Gomez, N., & DeConto, R. M. (2017). Variations of the Antarctic Ice Sheet in a Coupled Ice Sheet-Earth-Sea Level Model: Sensitivity to Viscoelastic Earth Properties. *Journal of Geophysical Research: Earth Surface*, *122*(11), 2124–2138. doi: 10.1002/2017JF004371

Rasmussen, C. E., & Williams, C. K. I. (2006). *Gaussian processes for machine learning (adaptive computation and machine learning)*. The MIT Press.

Rasmussen, D. J., Bittermann, K., Buchanan, M. K., Kulp, S., & Strauss, B. H. (2018). Extreme sea level implications of 1.5 C, 2.0 C, and 2.5 C temperature stabilization targets in the 21st and 22nd centuries. *Environmental Research Letters*, *13*.

Riahi, K., Rao, S., Krey, V., Cho, C., Chirkov, V., Fischer, G., ... Rafaj, P. (2011). RCP 8.5-A scenario of comparatively high greenhouse gas emissions. *Climatic Change*, *109*(1), 33–57. doi: 10.1007/s10584-011-0149-y

Rignot, E., Mouginot, J., van den Broeke, M., van Wessem, M. J., Morlighem, M., & Scheuchl, B. (2019). Four decades of Antarctic Ice Sheet mass balance from 1979–2017. *Proceedings of the National Academy of Sciences*, *116*(4), 1095–1103. doi: 10.1073/pnas.1812883116

Robel, A. A., Seroussi, H., & Roe, G. H. (2019). Marine ice sheet instability amplifies and skews uncertainty in projections of future sea-level rise. *Proceedings of the National Academy of Sciences*, 201904822. Retrieved from http://www.pnas.org/lookup/doi/10.1073/pnas.1904822116 doi: 10.1073/pnas.1904822116

Rohling, E. J., Grant, K., Hemleben, C., Siddall, M., Hoogakker, B. A. A., Bolshaw, M., & Kucera, M. (2008). High rates of sea-level rise during the last interglacial period. *Nature Geoscience*, *1*(1), 38–42. doi: 10.1038/ngeo.2007.28

Rovere, A., Raymo, M. E., Vacchi, M., Lorscheid, T., Stocchi, P., Gómez-Pujol, L., ... Hearty, P. J. (2016). The analysis of Last Interglacial (MIS 5e) relative sea-level indicators: Reconstructing sea-level in a warmer world. *Earth-Science Reviews*, *159*, 404–427. Retrieved from http://dx.doi.org/10.1016/j.earscirev.2016.06.006 doi: 10.1016/j.earscirev.2016.06.006

Scherer, R. P., Aldahan, A., Tulaczyk, S., Possnert, G., Engelhardt, H., & Kamb, B. (1998). Pleistocen collapse of the West Antarctic ice sheet. *Science*, *281*(5373), 82–85. doi: 10.1126/science.281.5373.82

Schoof, C. (2007). Ice sheet grounding line dynamics: Steady states, stability, and hysteresis. *Journal of Geophysical Research: Earth Surface*, *112*(3), 1–19. doi: 10.1029/2006JF000664

Seiyon Lee, B., Haran, M., Fuller, R., Pollard, D., & Keller, K. (2019, Mar). A Fast Particle-Based Approach for Calibrating a 3-D Model of the Antarctic Ice Sheet. *arXiv e-prints*, arXiv:1903.10032.

Silverman, B. W. (1986). *Density estimation for statistics and data analysis*. London: Chapman & Hall.

Solomon, S., Plattner, G.-K., Knutti, R., & Friedlingstein, P. (2009, feb). Irreversible climate change due to carbon dioxide emissions. *Proceedings of the National Academy of Sciences of the United States of America*, *106*(6), 1704–9. Retrieved from http://www.pubmedcentral.nih.gov/articlerender.fcgi?artid=2632717{\&}tool=pmcentrez{\&}rendertype=abstract doi: 10.1073/pnas.0812721106

Stammer, D., van de Wal, R., Nicholls, R., Church, J., Le Cozannet, G., Lowe, J.,

... Hinkel, J. (2019). Framework for high-end estimates of sea-level rise for stakeholder applications. *Earth's Future*, 1–16. doi: 10.1029/2019ef001163

Steig, E. J., & Neff, P. D. (2018). The prescience of paleoclimatology and the future of the Antarctic ice sheet. *Nature Communications*, *9*(1), 11–13. Retrieved from `http://dx.doi.org/10.1038/s41467-018-05001-1` doi: 10.1038/s41467-018-05001-1

Stocker, T., Qin, D., Plattner, G.-K., Alexander, L., Allen, S., Bindoff, N., ... Xie, S.-P. (2013). Technical summary [Book Section]. In T. Stocker et al. (Eds.), *Climate change 2013: The physical science basis. contribution of working group i to the fifth assessment report of the intergovernmental panel on climate change* (p. 33â115). Cambridge, United Kingdom and New York, NY, USA: Cambridge University Press. Retrieved from `www.climatechange2013.org` doi: 10.1017/CBO9781107415324.005

Weertman, J. (1974). Stability of the Junction of an Ice Sheet and an Ice Shelf. *Journal of Glaciology*, *13*(67), 3–11. doi: 10.3189/s0022143000023327

Wise, M. G., Dowdeswell, J. A., Jakobsson, M., & Larter, R. D. (2017). Evidence of marine ice-cliff instability in Pine Island Bay from iceberg-keel plough marks. *Nature*, *550*(7677), 506–510. Retrieved from `http://dx.doi.org/10.1038/nature24458` doi: 10.1038/nature24458

Wong, T. E., Bakker, A. M., & Keller, K. (2017). Impacts of Antarctic fast dynamics on sea-level projections and coastal flood defense. *Climatic Change*, *144*(2), 347–364. doi: 10.1007/s10584-017-2039-4

Zickfeld, K., Solomon, S., & Gilford, D. M. (2017). Centuries of thermal sea-level rise due to anthropogenic emissions of short-lived greenhouse gases. *Proceedings of the National Academy of Sciences*. Retrieved from `http://www.pnas.org/lookup/doi/10.1073/pnas.1612066114` doi: 10.1073/pnas.1612066114

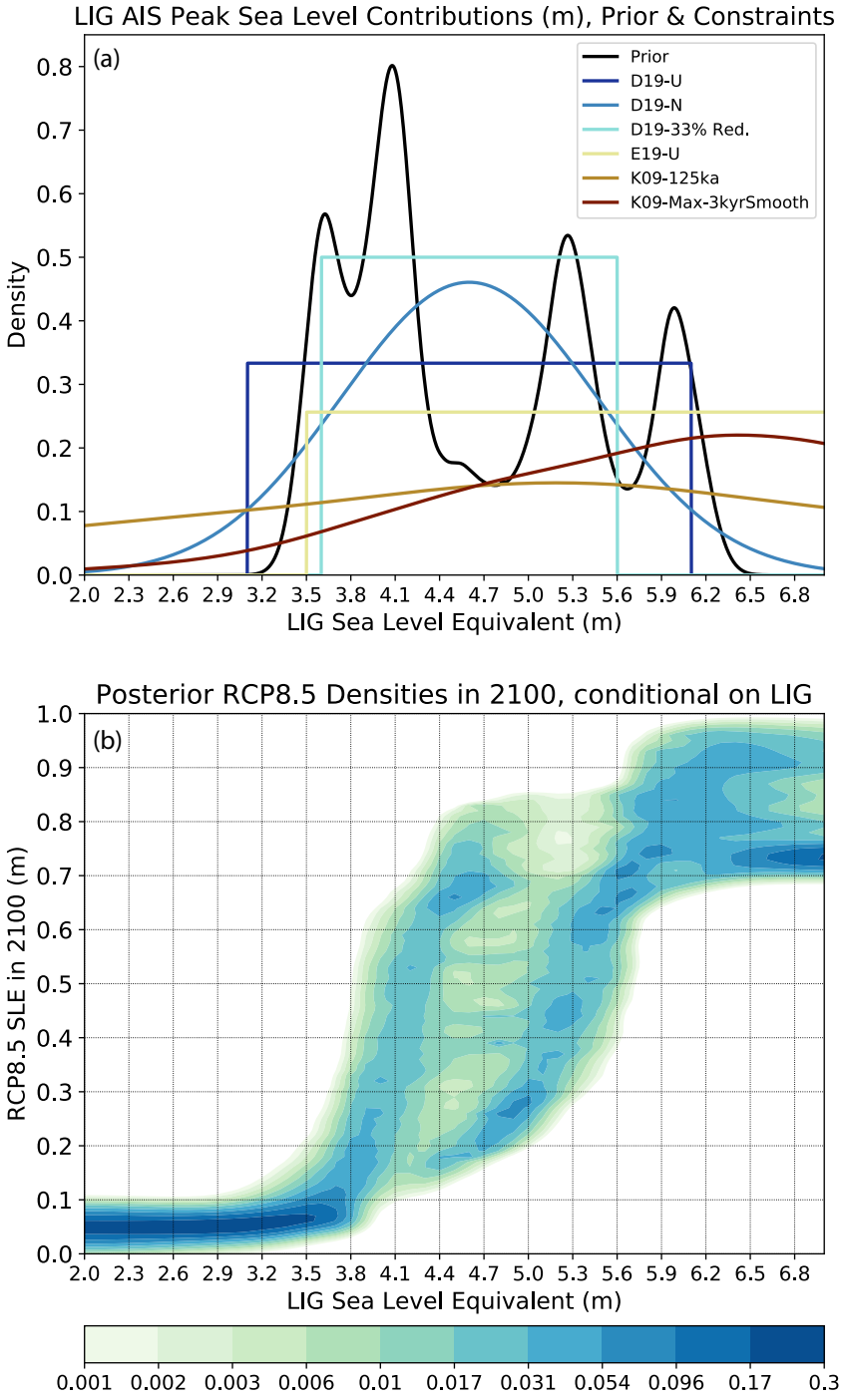


**Figure 4.** (a) Emulated prior (black curve) and specified constraints (colored curves) on last interglacial Antarctic ice sheet sea-level contributions. (b) Emulated probability densities of Antarctic ice sheet sea-level contributions in 2100 projected under an RCP8.5 scenario, conditional on emulated last interglacial contributions (bin widths of 10 cm).

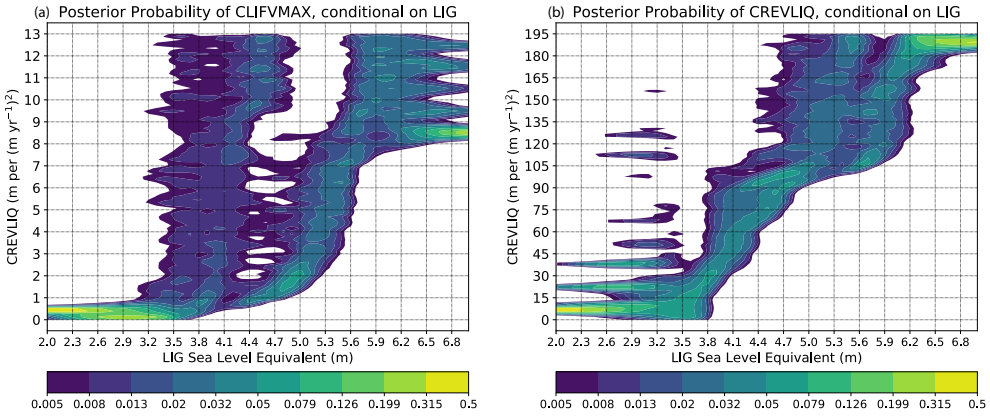


**Figure 5.** Emulated probability densities of marginal (a) CREVLIQ and (b) CLIFVMAX distributions, conditional on emulated last interglacial contributions (bins widths of 10 cm).

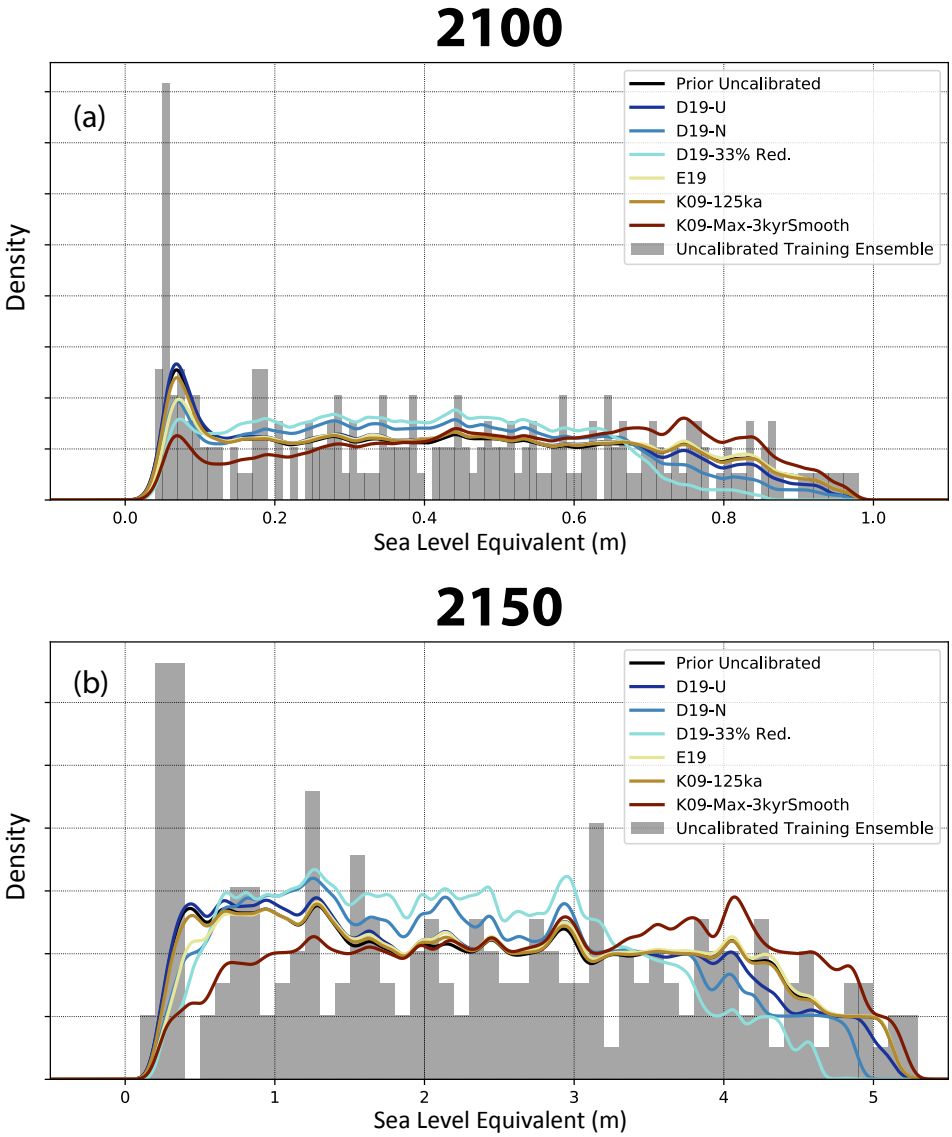


**Figure 6.** Probabilistic projections of emulated global mean sea-level contributions from Antarctica in (a) 2100 and (b) 2150, under an RCP8.5 scenario. Projection distributions from Latin-hypercube samples (lines) and estimated with kernel density estimation. Shown are the prior distribution with no constraints (black line), and distributions under specified constraints on last interglacial Antarctic ice sheet sea-level contributions (colored curves, cf. Figure 4). The training ensemble from the main text is shown as a histogram scaled for comparison.

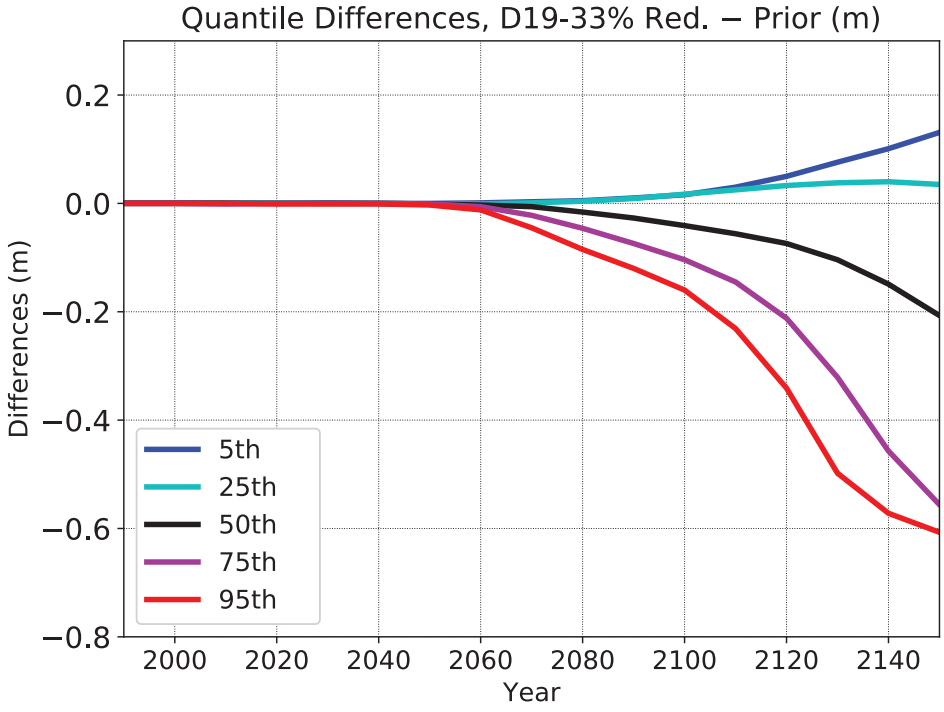


**Figure 7.** Differences between the distribution quantiles constrained by the D19-33% Red. LIG estimate and the emulator prior distribution.

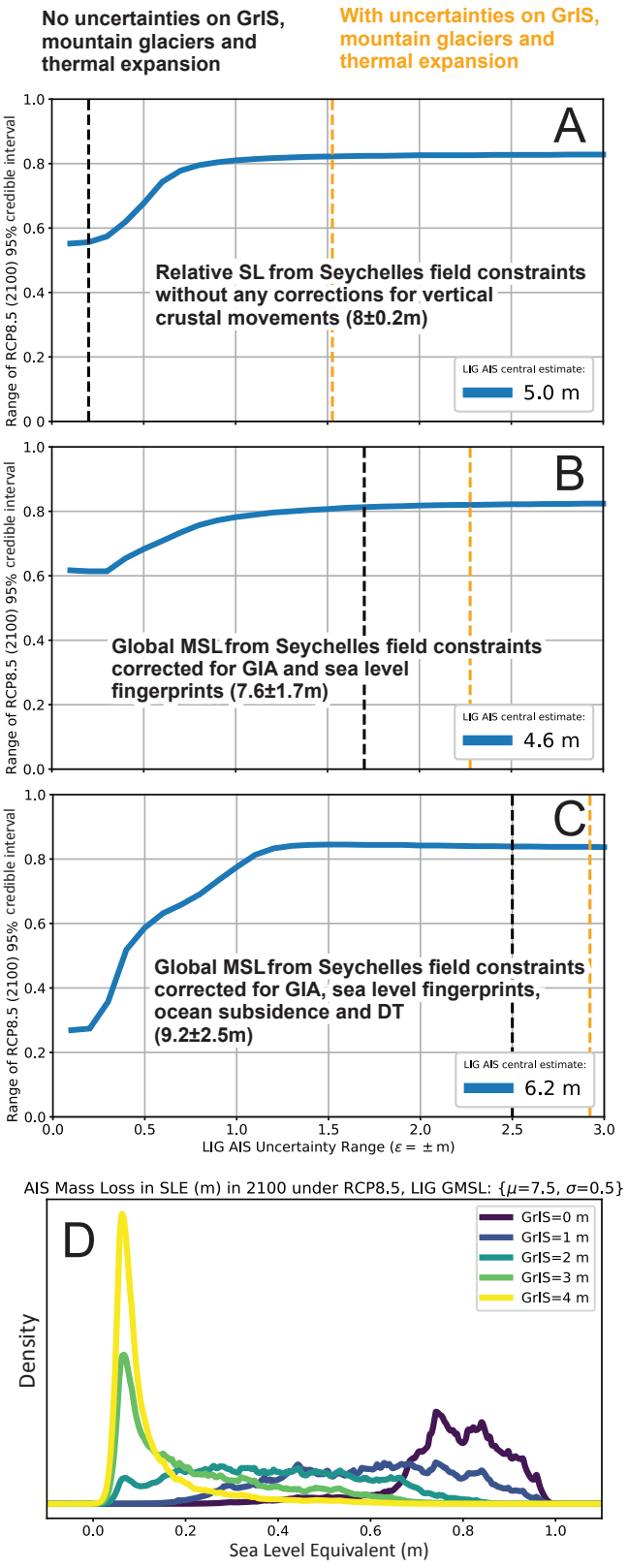


**Figure 8.** (A-C) Range of the 95% credible intervals of future AIS sea level contributions in 2100 under RCP8.5 forcing (m) conditional on three different scenarios of LIG AIS contributions with a central estimate (blue curves) and Gaussian $1\sigma$ uncertainties (see text); Combined total GriS and TMG mean contributions are taken to be 3 m. Black dashed curves show the total field uncertainties excluding those from GrIS and TMG contributions; orange dashed curves include GrIS and TMG uncertainties. (D) Probability density functions of AIS contributions in 2100 under RCP8.5 forcing, conditional on LIG global mean sea levels of 7.5±0.5 m, and mean GrIS sea-level contributions varying over 0-4 m.